scientific reports

Check for updates

OPEN

Projected changes in heatwaves over Central and South America using high-resolution regional climate simulations

M. V. S. Ramarao[1,11], Saravanan Arunachalam[1]✉, Brisa N. Sánchez[2], Leah H. Schinasi[2], Maryia Bakhtsiyarava[3], Waleska Teixeira Caiaffa[4], Iryna Dronova[5], Marie S. O'Neill[6], Ione Avila-Palencia[7], Nelson Gouveia[8], Yang Ju[3,9], Josiah L. Kephart[10] & Daniel A. Rodríguez[3]

Heatwaves (HWs) pose a severe threat to human and ecological systems. Here we assess the projected changes in heatwaves over Latin America using bias corrected high-resolution regional climate simulations under two Representative Concentration Pathway scenarios (RCPs). Heatwaves are projected to be more frequent, long-lasting, and intense in the mid-century under both RCP2.6 and RCP8.5 scenarios, with severe increases under the RCP8.5 scenario. Even under the low emissions scenario of RCP2.6, the frequency of heatwaves doubles over most of the region. A three- to tenfold rise in population exposure to heatwave days is projected over Central and South America, with climate change playing a dominant role in driving these changes. Results show that following the low emission pathway would reduce 57% and 50% of heatwave exposure for Central and South American regions respectively, highlighting the need to control anthropogenic emissions and implement sustainable practices.

Keywords Heatwave, Population exposure, Future scenarios, WRF modelling, High resolution climate projections, Latin America

Anthropogenic emissions and urbanization processes have led to a warming trend in global mean temperatures over the past few decades[1]. More specifically, global and regional observational studies have reported an increased number of heatwaves[2–7]. Heatwaves are episodes of extremely hot temperatures occurring in succession, leaving devastating impacts on natural and human-made ecosystems, including a higher propensity for wildfires, excess human mortality and morbidity, and regional economic losses, among other adverse outcomes[8–10]. The US Midwestern heatwaves of 1995 and 1999, the European heatwave of 2003[11], and severe heatwaves in Russia in 2010[12], India in 2015[13], and the Mediterranean Basin in 2021[14] are a sampling of well-documented recent mega heatwave events, which have resulted in great losses to human life. The earth's warmest year on record, 2023, had 20 more heatwave days reported than the yearly average from 1991 to 2020, leaving significant impacts on both Central and South America[15]. In addition, climate model simulations project a continued increase in heatwave frequency with the warming climate[16–21].

An understanding of region-specific projections of heatwaves under different emissions scenarios is critical to inform greenhouse gas emissions reduction and adaptation policies. These data may also be incorporated into models that project the future public health and economic impacts of rising temperatures, helping advise

[1]Institute for the Environment, The University of North Carolina at Chapel Hill, Chapel Hill, NC 27516, USA. [2]Department of Epidemiology and Biostatistics, Drexel Dornsife School of Public Health, Philadelphia, PA, USA. [3]Department of City and Regional Planning and Institute for Transportation Studies, University of California, Berkeley, CA, USA. [4]Observatory for Urban Health in Belo Horizonte, Federal University of Minas Gerais, Av. Pres. Antônio Carlos, 6627-Pampulha, Belo Horizonte 31270-901, MG, Brazil. [5]Department of Environmental Science, Policy and Management, Department of Landscape Architecture and Environmental Planning, University of California, Berkeley, CA 94720, USA. [6]Department of Environmental Health Sciences, University of Michigan School of Public Health, Ann Arbor, MI, USA. [7]Centre for Public Health, School of Medicine, Dentistry and Biomedical Sciences, Queen's University, Belfast, Northern Ireland, UK. [8]Department of Preventive Medicine, University of Sao Paulo Medical School, Sao Paulo, Brazil. [9]School of Architecture and Urban Planning, Nanjing University, Nanjing, China. [10]Urban Health Collaborative, Drexel Dornsife School of Public Health, Philadelphia, PA, USA. [11]National Centre for Medium Range Weather Forecasting, MoES, Noida, UP 201309, India. ✉email: sarav@email.unc.edu

policies, heat action plans, and warning systems[22]. Although prior heatwave projections have been based on state-of-the art global models, like those in the Coupled Model Intercomparison Project Phase 5 (CMIP5)[23], the coarse resolution (roughly 1 to 2 degrees) of these global models limits our understanding of future heatwave characteristics at regional and local scales. The inability of these models to resolve certain features, like topography and surface characteristics, is a setback to gaining better estimations of the projected changes in heatwave characteristics at regional scales. Dynamical downscaling, whereby coarse resolution global climate models (GCMs) are used to drive regional climate models (RCMs) at a higher resolution, can be applied to simulate heatwave occurrence and characteristics at regional scales. Several studies have used downscaled climate model projections available under the framework of Coordinated regional dynamical downscaling (CORDEX), including Europe[24], Africa[25], South America[26], and India[27]. These studies investigated the potential changes in heatwave characteristics over these regions with high spatial detail. The resolution of these downscaled simulations is approximately 50 km × 50 km, which is also considered to be coarser resolution than needed for performing impact assessment studies on the association between heatwaves and human mortality at local or urban scales. It should also be noted that such heatwave research has been largely concentrated in the Northern Hemisphere and remains limited in Southern Hemisphere, particularly in Latin America[26,28,29].

While there is growing evidence of the adverse impacts of extreme climatic events under anthropogenically driven climate change[30] (IPCC, 2022: Summary for policy makers), high-resolution information on future heatwaves and their potential risks to the human population is not available in Latin America. To address this gap, we investigate projected changes in heatwaves across the Latin American region in the mid-21st century using high-resolution (12 km × 12 km) downscaled regional climate simulations. Our analysis encompasses mid-21st century projections based on downscaled Weather Research and Forecasting model (WRF) simulations, under two future best-case and worse-case emissions scenarios as defined by the IPCC (RCP 2.6 and 8.5). Using high-resolution downscaled climate simulations, we provide a comprehensive assessment of changes in frequency, duration, and intensity of heatwaves, as well as changes in population exposure to heatwaves across Latin America under different warming scenarios. Future changes in population exposure depend on both changes in climate and in population distribution. To reflect these changes, we also disaggregate population exposure to understand the relative importance of climate, population drivers, and their interactions.

Results

Added value of regional climate simulation and heatwaves in base period

The spatial distribution of the annual mean daily temperature during the base period from WRF resembles that of ERA5L, with relatively hotter temperatures (around 25 °C) along the coastal regions of Central America (CAM) and tropical parts of South America (SAM), and cooler temperatures over the orographic regions of CAM and SAM and the southern parts of SAM, albeit with finer details everywhere (Supplementary Fig. S2). The spatial patterns of annual mean temperature display high correlations of about 0.96 and 0.98 over CAM and SAM domains. Still, the model shows cold bias over a large portion of Latin America and a warm bias (about 2 °C) over Argentina in Central South America (CSA) during the base period (Fig. 1a,c). The added value of the WRF simulations, compared to the CMIP5 MPI forcing over a significant portion of both the domains, is presented as hatching in Fig. 1a-d. This improvement in the high-resolution WRF simulation is likely due to the enhanced representation of complex dynamical processes at finer resolution. A significant reduction in this systematic bias is evident when comparing the bias-corrected WRF (WRF-BC) simulation against the raw WRF simulation, along with the enhancement in AV over the entire Latin America region (Fig. 1b,d). Similar reductions in bias and enhancement in AV over both domains is noted for seasonal mean temperatures and for temperature percentiles (Supplementary Figs. S3–S10). The bias correction has reduced bias throughout the temperature distribution and brought it closer to that of ERA5L over the larger CAM and SAM domains, as well as in specific sub-regions, as indicated by higher skill score (SS) for the WRF-BC outputs (Fig. 1e). We thus demonstrate that the bias-corrected, high-resolution downscaled simulations have added value by reducing bias in comparison to the driving model and increase confidence in the ability of these model outputs to identify heatwaves across Latin America.

The geographical distribution of heatwave metrics over Latin America from the WRF-BC simulation averaged for the base period is shown in Fig. 2. The spatial patterns of heatwave days per year (HWF), longest heatwave duration (HWD), and heatwave amplitude (HWA) reasonably match those obtained from ERA5L data (Supplementary Fig. S11) with pattern correlations of about 0.5, 0.5, and 0.9 for CAM and 0.7, 0.6, and 0.9 for SAM domains, respectively. A relatively higher HWF (> 14 days) is noted along western Mexico, Guatemala, and Nicaragua in CAM and over northern South America, eastern and central Brazil, along the western coasts of Peru and Chile in SAM. HWD indicates higher values over the same regions: > 7 days in CAM and > 12 days in SAM. Further comparison of the area averaged heatwave metrics of the model and ERA5L reveals that the model simulated HW metrics are comparable to those of ERA5L with a slight underestimation (Supplementary Table S1). This suggests that the bias-corrected WRF simulation is capable of capturing the present-day mean climate, temperature distribution, and number and geographical patterns of heatwave metrics realistically over the Latin America region.

Projected changes in heatwave characteristics

The spatial patterns of all projected HW metrics in Fig. 3 project increases in the future (2045–2054) under both RCP2.6 and RCP8.5 scenarios across Latin America. These scenarios show very similar qualitative results. HWs are expected be more frequent (HWN; Fig. 3i–l) and longer lasting (HWD; Fig. 3e–h), especially along the coastal regions of CAM and tropical northern regions of SAM like Amazon (AMZ) and CSA, with nearly a one to two degree rise in HWA (Fig. 3m–p). These incremental changes are more severe in RCP8.5 and expand over larger geographic areas. HW days per year (HWF, Fig. 3a–d) are also expected to rise significantly over these regions.

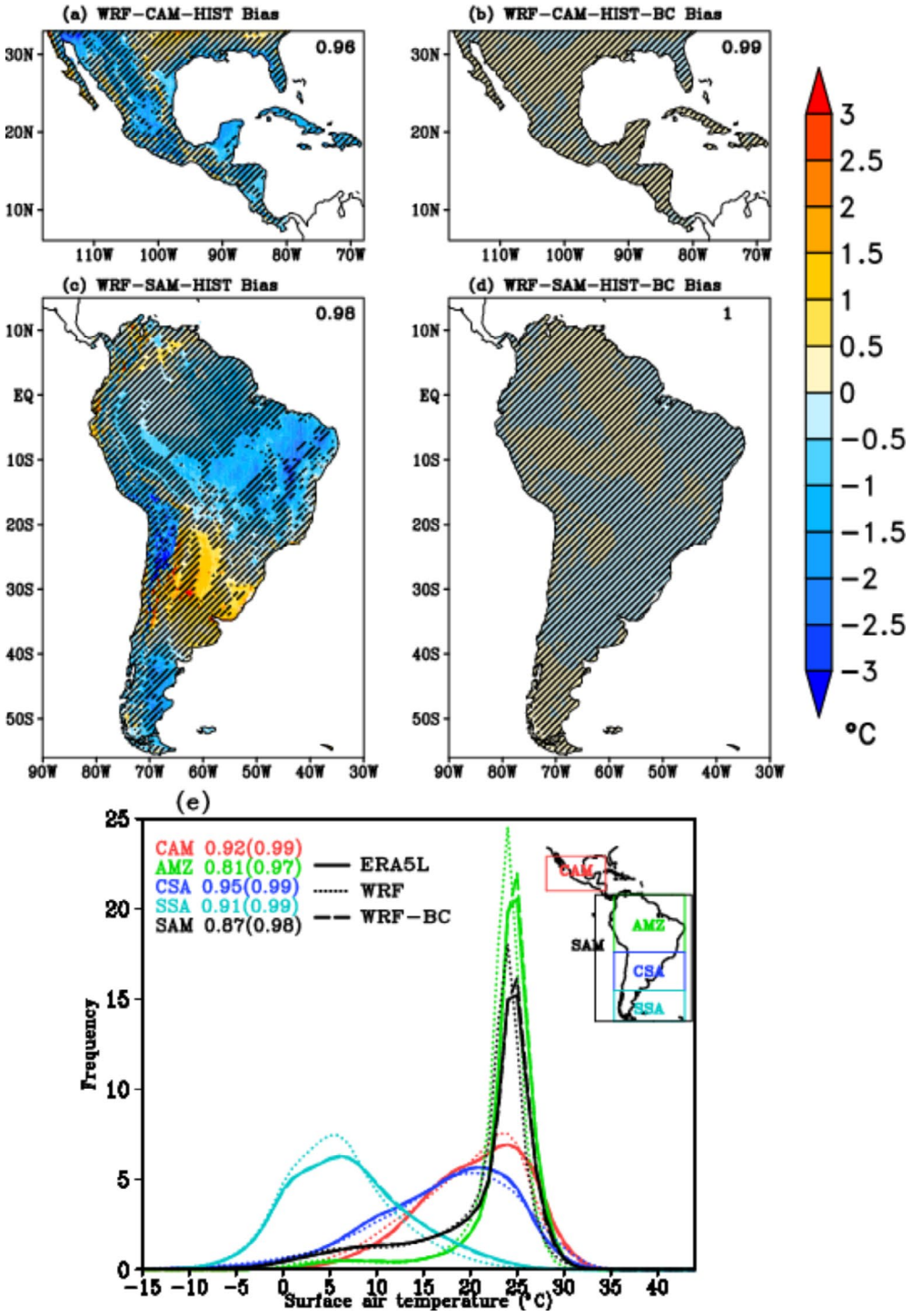

Fig. 1. Comparison of bias and distribution of temperature. Spatial pattern of bias in the annual mean temperature (°C) for (**a**,**b**) Central and (**c**,**d**) South America domains (first column) before and (second column) after applying bias correction during 1996–2005. Slanted lines indicate the grids where the WRF/WRF-BC simulation shows added value compared to the driving MPI simulation with lesser bias in temperature. Numerical values in each panel indicate the pattern correlations of mean temperature with ERA5L dataset. (e) Comparison of daily temperature distribution over various sub-regions of the Latin America (as indicated in the inset Figure) between the (dotted lines) WRF, (dashed lines) WRF-BC simulations and (solid lines) ERA5L dataset. Numerical values indicate the skill score of WRF (WRF-BC) against the ERA5L data. The boundaries of the subregions are as follows: Central America (CAM, 12–30 N; 120.5–83.5 W), Amazon (AMZ, 20 S–10 N; 78.5–34.5 W), Central South America (CSA, 40–20 S; 78.5–34.5 W), Southern South America (SSA, 56–40 S; 78.5–34.5 W) and South America (SAM, 56 S–10 N; 90–30 W). (This map was generated using GrADS (Version 2.1.a3), https://cola.gmu.edu/grads/).

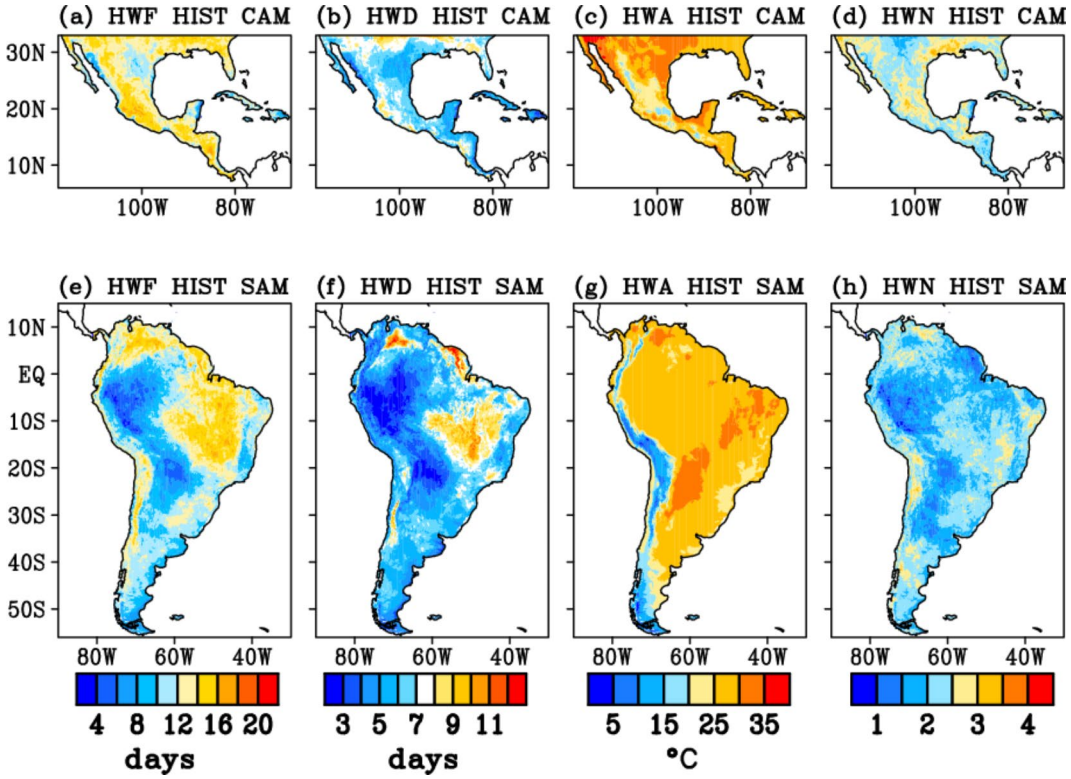

Fig. 2. Spatial distribution of HW metrics averaged for the base period 1996–2005 for (**a**–**d**) CAM and (**e**–**h**) SAM domains for (**a**,**e**) number of HW days, HWF; (**b**,**f**) longest HW duration, HWD; (**c**,**g**) HW amplitude, HWA and (**d**,**h**) number of HW events, HWN in a year from bias corrected WRF simulation. (This map was generated using GrADS (Version 2.1.a3), https://cola.gmu.edu/grads/).

Under the RCP2.6 scenario, HWF is expected to rise by 2.8, 4.5, 3, and 3.1-fold when averaged over CAM, AMZ, CSA, and SSA, respectively. HWD is also projected to increase by 2.5, 3.5, 2.4 and 2.1-fold over CAM, AMZ, CSA, and SSA, respectively, relative to HIST. These expected projections in HWF and HWD are much more severe under RCP8.5 (Table 1). The largest changes in HWF and HWD under RCP8.5 are expected over the AMZ region with 12 and 9.3-fold increases, respectively, while these increases in HW metrics are relatively less pronounced in SSA. HWN projections also exhibit similar regional features to both HWF and HWD estimates. The average number of HWs is expected to at least double in SSA, while they may increase 5-fold over the AMZ region (Table 1). Over the regions along the coastline of CAM, intra-America regions, western parts of AMZ, and along the coastline of northern SAM, more than 10-fold increases are projected (Fig. 3i-l). The geographical distribution and large increases in heatwave metrics over tropical regions of Central and South America are consistent with the findings of other regional and global studies[19,26,31,32] using projections under different RCPs at specific warming levels. Likewise, the projected increases in the average duration of a heatwave in a year (HWL) are also higher in the RCP8.5 scenario than in RCP2.6. The largest increase in the average duration of HWs is projected over AMZ under RCP8.5 (10-day increase), followed by CAM, CSA, and SSA sub-regions, with 4, 2, and 1-day increases in HWL, respectively (Supplementary Fig. S12).

Our findings at finer spatial resolution, with the model's systematic biases removed, are useful for identifying hotspot regions where immediate adaptation actions are needed. Greater increases in heatwave metrics over tropical areas are a function of increases in both mean temperature and temperature variability. Thus, even moderate increases in temperature in regions with low present-day variability and established seasonal cycles, like tropics, will result in longer heatwaves[21]. These severe changes in heatwave characteristics, along with other climate extremes like droughts[33], make ecologically sensitive regions like AMZ more vulnerable to the impacts of climate change.

We see that the mean temperature anomaly for the hottest day of the HW is expected to increase by about 1 °C across most of Latin America. Compared to the RCP8.5 scenario, the low emissions scenario of RCP2.6 will result in reductions in the number of heatwaves per year, ranging from 26 to 41% fewer HWs across the four sub-regions of Latin America. The reduction in HWF is about 30–62%, with the greatest reductions over the AMZ region. Similarly, the AMZ region under RCP2.6 is expected to experience 61% shorter heatwave durations compared to RCP8.5. These results indicate the importance of mitigation strategies to limit warming, which in turn will help reduce the severity of future heatwaves.

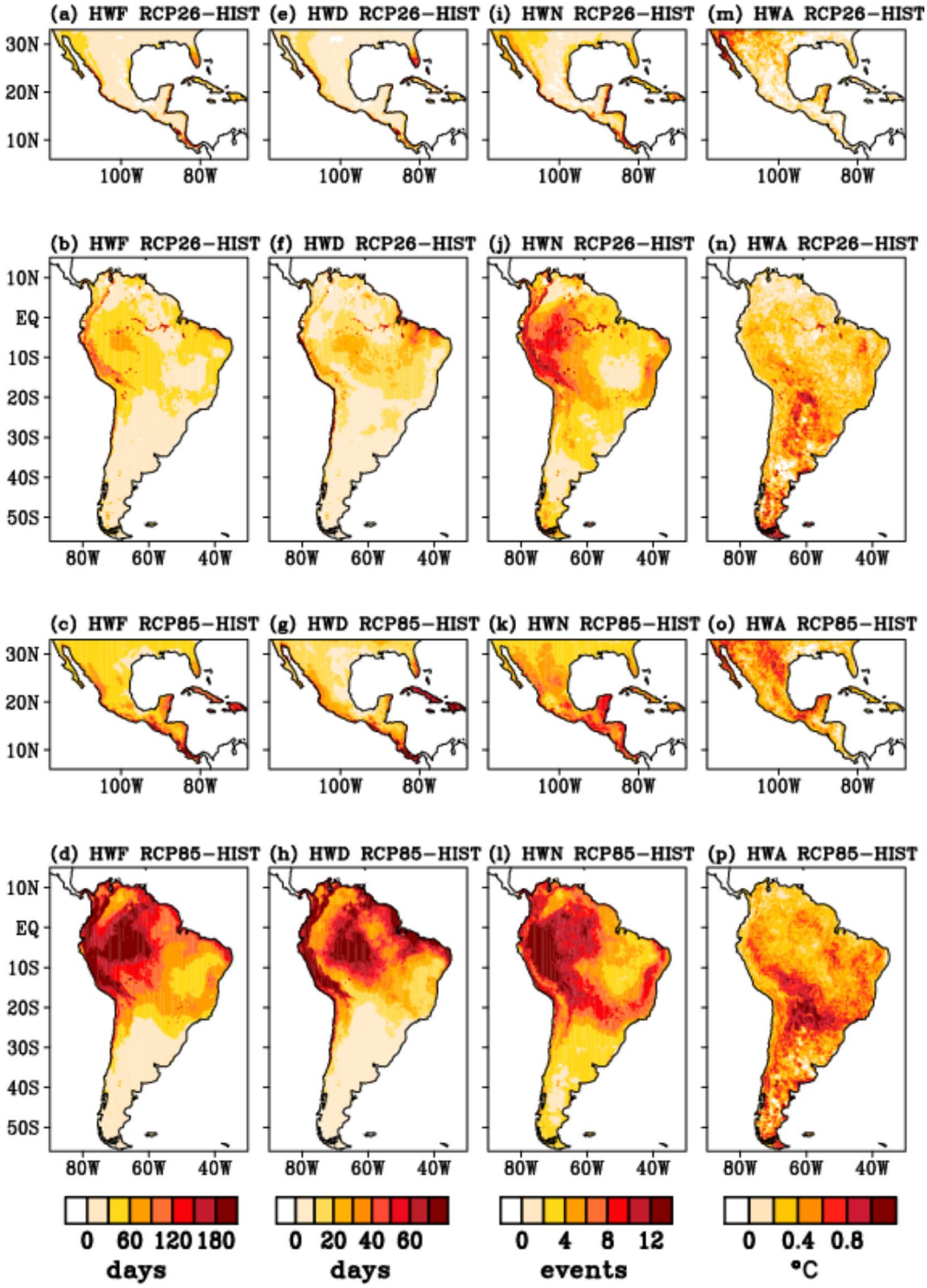

Fig. 3. **Projected changes in HW metrics over the period 2045–2054** under (first and second rows) RCP2.6 and (third and fourth rows) RCP8.5 scenarios for (a-d) HWF; (e-h) HWD; (i-l) HWN; (m-p) HWA. (This map was generated using GrADS (Version 2.1.a3), https://cola.gmu.edu/grads/).

Estimated changes in population exposure to heatwave days

The spatial distributions of population exposure to heatwave days over Latin America in the baseline period and the two future scenarios are similar. They are found to be highly spatially heterogeneous and concentrated over urban locations (Fig. 4). The geographic distribution of population exposure in the base period is found to be a combined effect of both population (Supplementary Fig. S13) and frequency of heatwave days (Fig. 2). In one example, the western coasts of Colombia, Ecuador, and northern Venezuela experience relatively fewer heatwave

Region	HWF			HWD			HWN		
	HIST	RCP26	RCP85	HIST	RCP26	RCP85	HIST	RCP26	RCP85
CAM	12.4	35(2.8)	68.5(5.5)	6.0	14.8(2.5)	23.7(3.9)	2.4	4.4(1.8)	7.5(3.1)
AMZ	11	50.3(4.6)	130(12)	5.7	20.1(3.6)	52.4(9.3)	1.9	6.3(3.2)	9.7(5)
CSA	10.2	30.9(3.0)	43.9(4.3)	5.5	13(2.4)	14.7(2.7)	2.0	4.5(2.3)	6.1(3.1)
SSA	9.5	29.8(3.1)	25.2(2.6)	5.1	10.3(2.1)	9.4(1.9)	2.2	4.9(2.3)	4.6(2.1)
SAM	10.7	44.6(4.1)	103(9.6)	5.6	18(3.2)	41.0(7.4)	2.0	5.8(2.9)	8.3(4.3)

Table 1. Comparison of area averaged HW metrics between HIST and two future scenarios RCP2.6 and RCP8.5. The numerical values in parentheses indicate the number of times in increase compared to the base period.

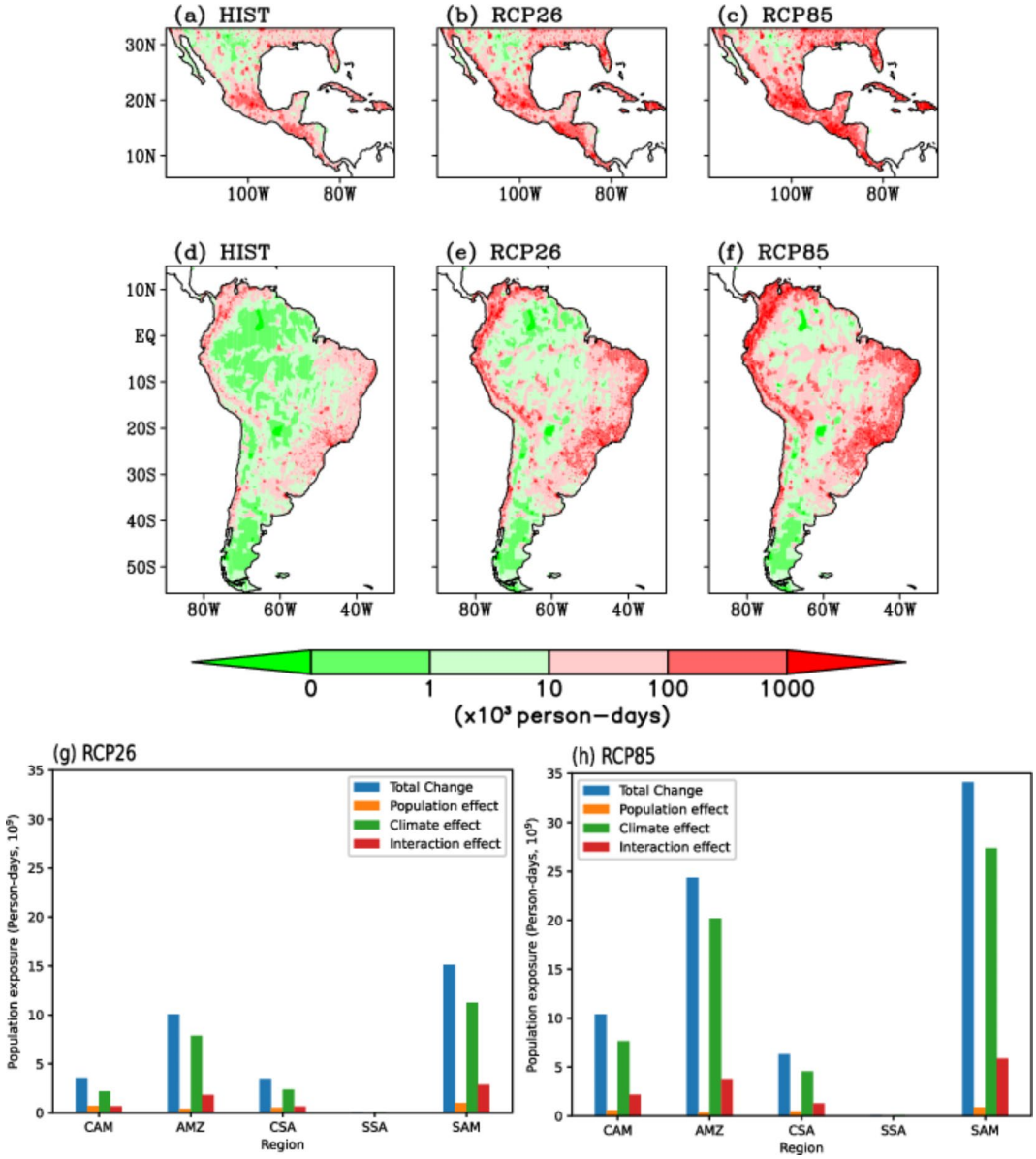

Fig. 4. Population exposure and determinants. Spatial distribution of population exposure for heatwave days in (**a**–**c**) CAM and (**d**–**f**) SAM domains for HIST, RCP2.6 and RCP8.5 simulations. (**g**,**h**) The total change in population exposure to heatwave days and its components under future scenarios. (This map was generated using GrADS (Version 2.1.a3), https://cola.gmu.edu/grads/).

days compared to the surrounding regions during the baseline period (Fig. 2a and e), but when combined with the high population in those regions, it results in higher population exposure (Fig. 4a-f). In a contrasting example, even though northern Mexico and parts of central Brazil experience a higher number of heatwave days, the population exposure is low due to the relatively lower population in those regions (Figs. 2 and 4 and Supplementary Fig. S13). Overall, areas with high population exposure are located in densely populated urban regions in Latin America. The aggregated annual population exposure in the base period is 1.7 and 3.6 billion-person days for the CAM and SAM domains, respectively. In the other sub regions of SAM, exposure is around 1.8, 1.5, and 0.019 billion-person days for AMZ, CSA and SSA, respectively.

Figure 4 also shows projected population exposure under RCP2.6-SSP1 and RCP8.5-SSP5 scenarios, with greater exposure under the high emissions scenario for the period 2045–2054. The aggregated average exposure is expected to reach 5.2 and 18.6 billion person-days for CAM and SAM under the low emissions scenario. The expected population exposure in absolute terms is about 11.8, 5.0, and 0.06 billion person-days for AMZ, CSA and SSA subregions, respectively. This represents a 3 and 5-fold increase in CAM and SAM domains, and a 6.5, 3.3, and 3.2-fold increase over AMZ, CSA, and SSA regions, compared to the baseline. As for the high emissions scenario, population exposure is expected to increase the most, reaching an aggregate value of 12.1 and 37.6 billion person-days for CAM and SAM domains. In relative terms, the increase in population exposure under RCP8.5-SSP5 would be around 7, 10.5, 14.4, 5.1, and 3-fold for CAM, SAM, AMZ, CSA and SSA, respectively, when compared to that of base period. In both scenarios, the increase in exposure is mainly concentrated around the urban locations, while the AMZ region is expected to experience the greatest change compared to the base period. At a larger spatial scale, achieving an RCP2.6-SSP1 future scenario, versus RCP8.5-SSP5, leads to roughly 6.9 and 19 billion fewer person-days of heatwave exposure for CAM and SAM, respectively. In relative terms, this is equal to a 57% and 50% of reduction in heatwave exposure for CAM and SAM regions. At the sub-regional scale, the avoided exposure under the low emissions scenario is 54.7% for AMZ and 36% for CSA. The SSA region does not show any difference in exposure to heatwave days between the two scenarios.

Future changes in population exposure depend on changes in both climate and population distribution. Figure 4g-h show the relative contributions of these drivers to the total change in population exposure for each sub-region under both scenarios. Overall, climate effects dominate the population and interaction effects: the order of contribution is climate effect > interaction effect > population effect in most of the regions under both scenarios. The relative contribution of climate varies across the sub regions, from 72 to 83% under RCP8.5-SSP5 and from 61 to 78% under RCP2.6-SSP1 combination scenarios. The contributions of interaction and population effects vary at 15.5–21% and 1.5–19.8% respectively across all regions and scenarios. For example, the largest increase in exposure is noted in the AMZ sub-region: the climate contribution dominates at around 83%, followed by the interaction effect at 15.5%, and the population effect at 1.5%. Over the CAM and CSA regions, the population and interaction effects have comparable contributions to total change under the low emissions scenario.

Discussion

This study investigates the projected changes in heatwave frequency, duration, and intensity over Latin America for 2045–2054 under two extreme emissions scenarios (RCP2.6 and RCP8.5) using high-resolution downscaled climate simulations. The downscaling by the regional climate model (WRF) and the use of bias correction add value by reducing biases in the simulated daily mean temperature and in temperature distribution across the region, compared to the driving global model (MPI-ESM-LR). The analysis of heatwaves of the base period climate (1996–2005) suggests that the bias-corrected model simulation captures the spatial patterns of the heatwave metrics realistically and is comparable to what is obtained from the ERA5L reanalysis dataset. Future projections indicate at least a doubling of heatwave events over a majority of the region under both RCP2.6 and RCP8.5 scenarios. The projected increases in HWF and HWD by mid-century range on the order of 2.6–12-fold and 1.8–9-fold, respectively, across the various sub-regions and two scenarios. As expected, these increases in HW metrics are more severe under the RCP8.5 scenario. The largest increases (12 and 9-fold) in HWF and HWD are expected to occur over the AMZ region under the RCP8.5 scenario. The geographic distribution and large increases in heatwave metrics over Latin America are largely consistent with the findings of other studies that used relatively coarser resolution model simulations[19,26,31,32]. These changes in heatwaves, along with other climate impacts, pose a severe threat to the ecologically sensitive Amazon region and its human population. Although both scenarios project large increases in heatwaves in the future, the low emissions scenario of RCP2.6 would result in 30–62% fewer HWF days across the region versus RCP8.5, potentially avoiding a substantial portion of the severe impacts of these events. In line with heatwave changes, population exposure to heatwave days is also expected to increase by about 61–83% across the sub-regions under the two modeled IPCC scenarios, with climate change as the strongest determinant in the increase in population heat exposure.

This study is based on a single model realization for a relatively short period (10 years), and only the two most extreme emissions scenarios were considered due to computational burden. Despite this, the greater realism of the high-resolution simulation, compared to coarser resolution GCM simulations, enhances our confidence in understanding heatwave characteristics and population exposure in a changing climate at different scales. In our study, we used only RCP2.6-SSP1 and RCP8.5-SSP5 combinations of emissions (RCPs) and population (SSPs) scenarios to explore population exposure, while other combinations of these two extreme emissions scenarios may also be possible. We also realize that the use of other population scenarios could provide differing estimates of population exposure and relative contributions, such as SSP3, which has the largest increase in population and could pose great challenges to mitigation and adaptation[34]. However, our high-resolution simulations provide reliable estimates of projected heatwave changes. They are useful in exploring the actual risks associated with heatwaves, especially in terms of heat-mortality relations, as documented at the city level[35]. This is an important topic of interest for future studies. It should be noted that since this work is based on only a single model

realization, the results will not reveal the uncertainty associated with changes in heatwaves. Past studies have revealed that model spread in simulating global mean temperature changes is lower around the middle of the century than at the end of the century[36]. We found that the model-projected changes in heatwave characteristics in the current study are comparable with the results of previous studies, hence giving confidence in the robustness of our findings.

Our results are particularly relevant as we present a high-resolution analysis of changes in heatwaves, along with population exposure to heatwave days, over the relatively less studied and highly vulnerable region of Latin America. We also show that following the low emissions scenario leads to 57% and 50% lower exposure to heatwaves at larger geographical scales for CAM and SAM regions. There is thus a need for immediate action to develop better emissions reduction strategies and accelerate mitigation efforts in order to minimize the adverse effects of heatwaves on the Latin American region.

Methods

Regional climate downscaling using WRF and bias correction

We dynamically downscale one historical period and two future projections from a single earth system model (ESM), specifically the low-resolution version of Max-Planck-Institute Earth System Model (MPI-ESM-LR; referred as MPI hereafter)[37] from CMIP5 at 12 km × 12-km horizontal resolution over Latin America using WRF model v4.1.4[38]. WRF model was configured for two smaller domains over Latin America: Central America including Mexico (CAM) and South America (SAM) (Supplementary Fig. S1). Three downscaled simulations were run for each domain: one for historical period (1996–2005; HIST) and two future simulations (2045–2054) following two extreme Intergovernmental Panel on Climate Change (IPCC) approved future scenarios. These scenarios are Representative Concentration Pathway 2.6 (RCP 2.6) and 8.5 (RCP 8.5). Further details on model simulations and the selection of the driving model are provided in supplementary information (Supplementary Notes).

We further applied a statistical bias correction, which adds a constant offset factor to correct for the differences between the simulated and observed monthly mean temperature in the historical period at each grid point[39]. This method also modifies the daily variability of the simulated temperature data around their monthly means to match the observed daily variability in the historical period (1996–2005). The same offset factors were then applied to the future period of the model simulation (2045–2054). This method has been developed within the widely used Inter-Sectoral Impact Model Intercomparison Project (ISI-MIP)[40], which was designed to project the impacts of climate change across sectors like agriculture, water, biome, and health. We used hourly temperature data at 9 km × 9 km horizontal resolution available from a recently released reanalysis from the European Centre for Medium-Range Weather Forecasts (ECMWF), namely the land component of the fifth generation of European ReAnalysis (ERA5L)[41], as the reference dataset. Model outputs were bilinearly interpolated to ERA5L grids before applying bias correction.

The added value (AV) of the WRF simulations against the driving MPI global model for the mean climate and various percentile thresholds of 2 m air temperature were verified by comparing the squared errors of RCM and GCM with respect to the ERA5L dataset[42]. We used the AV metric[42], which compares the squared errors of RCM and GCM with respect to observations. This AV metric was later adopted by many regional climate studies to show the value addition of regional climate simulations against the driving global models. The formula for AV is as follows:

$$AV = \frac{(X_{GCM} - X_{OBS})^2 - (X_{RCM} - X_{OBS})^2}{Max\left((X_{GCM} - X_{OBS})^2, (X_{RCM} - X_{OBS})^2\right)} \quad (1)$$

where X represents the simulated variable from the driving model (GCM i.e., MPI in our case), regional model (RCM, i.e., WRF in our case), and observations (OBS, i.e., ERA5L in our case). The normalization with the max value of squared errors of GCM and RCM confines the AV value between −1 and 1. Here, the positive value of AV indicates that the square error of MPI is higher than that of WRF and hence indicates the value addition of the RCM.

We further compared the skill of RCM and GCM against the observed distribution of 2 m air temperature over the Latin America region at a daily scale. We used a simple metric proposed by Perkins et al. [43] which measures the closeness of the empirical distributions of model simulated daily 2 m air temperature and that of observations. We first constructed the empirical probability distribution functions by binning the temperature data in N bins with 0.5 ˚C bin width and then computed the Skill Score (SS) between model and observation datasets as

$$SS = \sum_{1}^{N} min\left(Z_m, Z_o\right) \quad (2)$$

where N is the number of bins and Z_m and Z_o are the frequency of the values in the given bin for model and observations, respectively. An SS value of one represents two distributions matching perfectly, and a value near zero represents a weak overlap of the two distributions. The spatial correlations are calculated between the model simulated and ERA5L datasets for the mean temperature. The significance level of the correlation coefficient was calculated based on the two-tailed Student's t-test. The spatial correlation coefficients with values $> \pm 0.30$ are significant at 95% confidence level.

Heatwave identification

Even though a universal definition of heatwave does not exist, most studies define a heatwave as a period of excessively hot temperatures persisting over a prolonged period, typically 3 or more days[6,27]. In this study, we use the definition of Excess Heat Factor (EHF)[44] to identify heatwaves. This index is based on two excess heat indices. The first excess heat index, called the significance index, measures how hot a three-day period is relative to the 95th percentile of temperature for the given time period and is computed as:

$$EHI\ (sig) = \left[(T_i + T_{i-1} + T_{i-2})/3\right] - T_{95} \tag{3}$$

where T_i is the average daily temperature for the day i and T_{95} is the 95th percentile of temperature distribution over the given period (1996–2005 in our case).

The second excess heat index, called the acclimatization index, measures the temperature anomaly over a 3-day period against the preceding 30 days and can be computed as follows:

$$EHI\,(accl) = \left[(T_i + T_{i-1} + T_{i-2})/3\right] - \left[(T_{i-3} + \ldots + T_{i-32})/30\right] \tag{4}$$

Equations (3) and (4) are then combined to derive EHF as follows:

$$EHF = max\left[1, EHI\,(accl)\right] \times\ EHI\,(sig) \tag{5}$$

where the positive values of EHF indicate heatwave conditions for day *i*. Per Eq. (4), for a given day the temperature is compared to an extreme threshold (95th percentile) to determine its climatological anomaly. It is also compared to the mean of the preceding month to determine the temperature anomaly against recent conditions, which indicates acclimatization to the heatwave conditions. A heatwave is considered to occur if positive conditions of EHF are observed consecutively for three days or more.

Furthermore, we used four HW metrics:

(1) HW amplitude (HWA): temperature anomaly (in °C) of the hottest day of any HW during a year.
(2) HW duration (HWD): the length (in days) of the longest HW during a year.
(3) HW frequency (HWF): number of HW days per year, and.
(4) Number of HWs per year (HWN).

We computed these heatwave characteristics for both base and future periods from model simulations, and changes in future heatwave characteristics were computed as differences between the future and current climate. In addition, we have also computed the average duration of HW in a year (HWL) for base and future periods.

The baseline (year 2000) and projected population data sets corresponding to future climate and socioeconomic scenarios come from Shared Socioeconomic Pathways (SSPs), which was developed by Socioeconomic Data and Applications Center (SEDAC). These are available at ten-year intervals from 2010 to 2100 and at a resolution of 1 km × 1 km on global land[45]. These were used for estimating the changes in population exposure. The SSPs and RCPs are closely tied and applied to project future scenarios of socioeconomic development[34]. We thus used the projected population changes for SSP1 and SSP5 scenarios, which are closely linked to the low and high emissions scenarios of RCP2.6 and RCP 8.5, respectively. Population exposure to heatwave days was computed by multiplying the population at each grid point with the 10-year average number of heatwave days in both the base period and future period for each scenario. The units for population exposure are person-days. The difference between the future and base period exposures represents the projected changes in population exposure to heatwave days. The changes in population exposure were further decomposed into the impact of climate change (keeping population constant), the impact of population change (keeping the climate impact as that of the base period), and the impact due to the interaction of both climate change and population change following[17] as follows:

$$\Delta\, PE = P_{base} \times\ \Delta\, C + C_{base} \times\ \Delta\, P + \ Interaction(P, C) \tag{6}$$

where $\Delta\, PE$ is the total change in population exposure to heatwaves and C_{base} and P_{base} are the annual mean number of heatwave days and population in the base period, respectively. $\Delta\, P$ and $\Delta\, C$ are the change in population and change in annual mean number of heatwave days from the base period to the future period. Finally, the interaction effect was computed as the difference between the total change in population exposure and the sum of the population and climate impacts.

Data availability

The WRF high resolution climate simulations used in this study are generated at UNC computing facilities. The datasets used and analyzed in the current study are available from the corresponding author upon reasonable request. ERA5L dataset is freely available from https://cds.climate.copernicus.eu/cdsapp#!/dataset/reanalysis-era5-land? tab=form.

Received: 6 May 2024; Accepted: 18 September 2024
Published online: 04 October 2024

References

1. Eyring, V. et al. Human influence on the climate system. In *Climate Change 2021: The Physical Science Basis. Contribution of Working Group I to the Sixth Assessment Report of the Intergovernmental Panel on Climate Change* 423–552 (Cambridge University Press, 2023). https://doi.org/10.1017/9781009157896.005.
2. Frich, P. et al. Observed coherent changes in climatic extremes during the second half of the twentieth century. *Clim. Res.* **19**, 193–212 (2002).
3. Perkins, S. E., Alexander, L. & Nairn, J. R. Increasing frequency, intensity and duration of observed global heatwaves and warm spells. *Geophys. Res. Lett.* **39**, 20714 (2012).
4. Sun, X. et al. Effects of temperature and heat waves on emergency department visits and emergency ambulance dispatches in Pudong New Area, China: a time series analysis. *Environ. Health* **13**, 1–8 (2014).
5. Russo, S., Sillmann, J. & Fischer, E. M. Top ten European heatwaves since 1950 and their occurrence in the coming decades. *Environ. Res. Lett.***10**, 124003 (2015).
6. Rohini, P., Rajeevan, M. & Srivastava, A. K. On the variability and increasing trends of Heat waves over India OPEN (2016). https://doi.org/10.1038/srep26153.
7. Wuebbles, D. J. et al. Executive summary. Climate Science Special Report: Fourth National Climate Assessment. **I**, 12–34 (2017). https://doi.org/10.7930/J0DJ5CTG.
8. Ebi, K. L. et al. Hot weather and heat extremes: health risks. *Lancet*. **398**, 698–708 (2021).
9. Ballester, J. et al. Heat-related mortality in Europe during the summer of 2022. *Nat. Med.* **29**, 1857–1866 (2023).
10. Zhao, Q. et al. Global, regional, and national burden of mortality associated with non-optimal ambient temperatures from 2000 to 2019: a three-stage modelling study. *Lancet Planet. Health*. **5**, e415–e425 (2021).
11. Schär, C. et al. The role of increasing temperature variability in European summer heatwaves. *Nature*. **427**, 332–336 (2004).
12. Trenberth, K. E. & Fasullo, J. T. Climate extremes and climate change: the Russian heat wave and other climate extremes of 2010. *J. Geophys. Res. Atmos.* **117**, 17103 (2012).
13. Ghatak, D., Zaitchik, B., Hain, C. & Anderson, M. The role of local heating in the 2015 Indian Heat Wave. *Sci. Rep.* **7**, 1–8 (2017).
14. Lhotka, O. & Kyselý, J. The 2021 European Heat Wave in the context of past major heat waves. *Earth Space Sci.* **9**, e2022EA002567 (2022).
15. Perkins-Kirkpatrick, S. et al. Extreme terrestrial heat in 2023. *Nat. Rev. Earth Environ.* **5**, 244–246 (2024).
16. Lau, N. C. & Nath, M. J. Model simulation and projection of european heat waves in present-day and future climates. *J. Clim.* **27**, 3713–3730 (2014).
17. Jones, B. et al. Future population exposure to US heat extremes. *Nat. Clim. Chang.* **5** (2015).
18. Schär, C. The worst heat waves to come. *Nat. Clim. Change*. **6** (2), 6–128 (2015).
19. Russo, S., Sillmann, J. & Sterl, A. Humid heat waves at different warming levels. *Sci. Rep.* **7**, 1–7 (2017).
20. Oleson, K. W., Anderson, G. B., Jones, B., McGinnis, S. A. & Sanderson, B. Avoided climate impacts of urban and rural heat and cold waves over the U.S. using large climate model ensembles for RCP8.5 and RCP4.5. *Clim. Change*. **146**, 377–392 (2018).
21. Dosio, A., Mentaschi, L., Fischer, E. M. & Wyser, K. Extreme heat waves under 1.5°C and 2°C global warming. *Environ. Res. Lett.* **13**, 054006 (2018).
22. Kendrovski, V. et al. Quantifying projected heat mortality impacts under 21st-Century warming conditions for selected European countries. *Int. J. Environ. Res. Public. Health 2017*. **14**, 729 (2017).
23. Taylor, K. E., Stouffer, R. J. & Meehl, G. A. An overview of CMIP5 and the experiment design. *Bull. Am. Meteorol. Soc.* **93**, 485–498 (2012).
24. Jacob, D. et al. EURO-CORDEX: New high-resolution climate change projections for European impact research. *Reg. Environ. Change*. **14**, 563–578 (2014).
25. Nikulin, G. et al. Precipitation climatology in an ensemble of CORDEX-Africa regional climate simulations. *J. Clim.* **25**, 6057–6078 (2012).
26. Feron, S. et al. Observations and projections of heat waves in South America. *Sci. Rep.* **9**, 8173 (2019).
27. Sanjay, J. et al. Temperature changes in India. *Assessment of Climate Change over the Indian Region: A Report of the Ministry of Earth Sciences (MoES), Government of India* 21–45(2020). https://link.springer.com/chapter/10.1007/978-981-15-4327-2_2.
28. Miranda, V. F. V. V. et al. Heat stress in South America over the last four decades: a bioclimatic analysis. *Theor. Appl. Climatol.* **155**, 911–928 (2024).
29. Kephart, J. L. et al. City-level impact of extreme temperatures and mortality in Latin America. *Nat. Med.* **28**, 1700–1705 (2022).
30. Langsdorf, S., Löschke, S., Möller, V. & Okem, A. Climate Change 2022 Impacts, Adaptation and Vulnerability Working Group II Contribution to the Sixth Assessment Report of the Intergovernmental Panel on Climate Change. (2022).
31. Russo, S. et al. Magnitude of extreme heat waves in present climate and their projection in a warming world. *J. Geophys. Res. Atmos.* **119**, 12500–12512 (2014).
32. Mora, C. et al. Global risk of deadly heat. *Nat. Clim. Change* **7**, 501–506 (2017).
33. Duffy, P. B., Brando, P., Asner, G. P. & Field, C. B. Projections of future meteorological drought and wet periods in the Amazon. *Proc. Natl. Acad. Sci. U. S. A.*. **112**, 13172–13177 (2015).
34. O'Neill, B. C. et al. The roads ahead: narratives for shared socioeconomic pathways describing world futures in the 21st century. *Glob. Environ. Change*. **42**, 169–180 (2017).
35. Gasparrini, A. et al. Projections of temperature-related excess mortality under climate change scenarios. *Lancet Planet. Health*. **1**, e360–e367 (2017).
36. Sillmann, J., Kharin, V. V., Zwiers, F. W., Zhang, X. & Bronaugh, D. Climate extremes indices in the CMIP5 multimodel ensemble: part 2. Future climate projections. *J. Geophys. Res. Atmos.* **118**, 2473–2493 (2013).
37. Giorgetta, M. A. et al. Climate and carbon cycle changes from 1850 to 2100 in MPI-ESM simulations for the coupled model Intercomparison Project phase 5. *J. Adv. Model. Earth Syst.* **5**, 572–597 (2013).
38. Skamarock, W. C. et al. A description of the Advanced Research WRF Model Version 4.1. doi: (2019). https://doi.org/10.5065/1DFH-6P97
39. *Earth Syst. Dyn.* **4**, 219–236 (2013).
40. Warszawski, L. et al. The inter-sectoral impact model intercomparison project (ISI–MIP): Project framework. *Proc. Natl. Acad. Sci.* **111**, 3228–3232 (2014).
41. Muñoz-Sabater, J. et al. ERA5-Land: a state-of-the-art global reanalysis dataset for land applications. *Earth Syst. Sci. Data*. **13**, 4349–4383 (2021).
42. Akinsanola, A. A. & Zhou, W. Projection of west African summer monsoon rainfall in dynamically downscaled CMIP5 models. *Clim. Dyn.* **53**, 81–95 (2019).
43. Perkins, S. E., Pitman, A. J., Holbrook, N. J. & McAneney, J. Evaluation of the AR4 climate models' simulated daily Maximum temperature, Minimum temperature, and precipitation over Australia using probability density functions. *J. Clim.* **20**, 4356–4376 (2007).
44. Nairn, J. R. & Fawcett, R. J. B. The excess heat factor: a metric for heatwave intensity and its use in classifying heatwave severity. *Int. J. Environ. Res. Public. Health*. **12**, 227–253 (2014).
45. Gao, J. N. C. A. R. & Technical Notes NCAR/TN-537 + STR downscaling global spatial Population projections from 1/8-degree to 1-km Grid cells Jing Gao. *NCAR Tech. Notes* (2017).

Acknowledgements
The authors acknowledge the contribution of all SALURBAL project team members. For more information on SALURBAL and to see a full list of investigators see https://drexel.edu/lac/salurbal/team/. The Salud Urbana en América Latina (SALURBAL)/ Urban Health in Latin America project is funded by the Wellcome Trust [205177/Z/16/Z].

Author contributions
R.M.: conceptualization, methodology, modelling, formal analysis, writing - original draft, writing—review and editing, visualization. S.A.: conceptualization, supervision, writing—review and editing. All other authors have equally contributed to discussions and writing—review and editing. All authors read and approved the final manuscript.

Declarations

Competing interests
The authors declare no competing interests.

Additional information
Supplementary Information The online version contains supplementary material available at https://doi.org/10.1038/s41598-024-73521-6.

Correspondence and requests for materials should be addressed to S.A.

Reprints and permissions information is available at www.nature.com/reprints.

Publisher's note Springer Nature remains neutral with regard to jurisdictional claims in published maps and institutional affiliations.